

Hydrogen Molecule in the Small Dodecahedral Cage of a Clathrate Hydrate: Quantum Translation–Rotation Dynamics at Higher Excitation Energies[†]

Minzhong Xu, Francesco Sebastianelli, and Zlatko Bačić*

Department of Chemistry, New York University, New York, New York 10003

Received: August 6, 2007; In Final Form: September 11, 2007

Higher-lying five-dimensional translation–rotation (T–R) eigenstates of a single *p*-H₂ and *o*-D₂ molecule confined inside the small dodecahedral (5¹²) cage of the structure II clathrate hydrate are calculated rigorously, as fully coupled, with the cage assumed to be rigid. The calculations cover the excitation energies up to and beyond the *j* = 2 rotational level of the free molecule, 356 cm^{−1} for H₂ and 179 cm^{−1} for D₂. It is found that *j* is a good quantum number for all the T–R states of *p*-H₂, *j* = 0 and *j* = 2, considered. The same is not true for *o*-D₂, where a number of T–R states in the neighborhood of the *j* = 2 level show significant mixing of *j* = 0 and *j* = 2 rotational basis functions. The 5-fold degeneracy of the *j* = 2 level of *p*-H₂ is lifted completely due to the anisotropy of the cage environment, as is the 3-fold degeneracy of the *j* = 1 level of *o*-H₂ studied by us previously. Pure translational mode excitations with up to four quanta display negative anharmonicity, which was observed earlier for the translational fundamentals and their first overtones. The issues of assigning the combination states of *p*-H₂ with excitations of two or all three translational modes, and of the strength of the mode coupling as a function of the excitation energy, are studied carefully for a range of quantum numbers. The average T–R energy of the encapsulated *p*-H₂ is calculated as a function of temperature from 0 to 150 K.

I. Introduction

Clathrate hydrates are crystalline inclusion compounds formed, typically at low temperature and elevated pressure, when guest molecules of suitable shape and size are enclosed inside the polyhedral cavities within the framework of hydrogen-bonded water molecules.¹ Historically, hydrogen molecules were considered to be too small to stabilize clathrate hydrates. But, this view underwent a revision several years ago, when a clathrate hydrate with hydrogen molecules as guests was synthesized under very high pressures and low temperatures, typically 180–220 MPa at around 249 K.² This hydrogen hydrate adopts the classical structure II (sII), whose unit cell has 16 pentagonal dodecahedron (5¹²) small cages comprised of 20 H₂O molecules and 8 hexakaidecahedron (5¹²6⁴) large cages formed by 28 H₂O molecules. Initial studies reported double occupancy of H₂ in the small 5¹² cage and quadruple H₂ occupancy in the large 5¹²6⁴ cage.² This finding suggested that the hydrogen hydrate might be a promising hydrogen storage material,^{3–5} motivating numerous further studies of pure H₂^{6,7} and binary clathrate hydrates.^{8–14} In the subsequent neutron diffraction experiments on the pure sII hydrogen hydrate⁶ only one D₂ molecule was found in the small cage, and up to four D₂ molecules in the large cage. Single occupancy of D₂ in the small cage was confirmed also for the binary sII clathrate hydrate with tetrahydrofuran (THF) as the second guest, in high-resolution neutron diffraction experiments¹¹ and the hydrogen-storage capacity studies.¹²

Pure H₂^{15–20} and binary H₂–THF clathrate hydrate²¹ have been the subject of numerous theoretical studies. These were mainly concerned with the issue of the thermodynamic stability of the

clathrates as a function of the number of H₂ molecules in the small and large cages. In these investigations, the treatment of the dynamics of the encapsulated hydrogen molecules was limited to classical molecular dynamics simulations.

However, the dynamics of one or more light hydrogen molecules inside the clathrate cage, large or small, at the low temperatures of experimental interest, is highly quantum mechanical, due to the large zero-point energy of their coupled translational and rotational motions and extensive wave function delocalization. Consequently, classical mechanics cannot provide a qualitatively correct, let alone quantitative, description of the dynamical properties of hydrogen hydrates. Prior to our recent work outlined below, in only one instance,¹⁷ the motion of H₂ inside the small dodecahedral cage was treated by solving the textbook one-dimensional (1D) Schrödinger equation for the bound states of a structureless particle in a spherically symmetric potential. This 1D approach leaves out completely the rotational eigenstates of the H₂ molecule, which are probed directly in the Raman spectroscopy of the pure H₂² and the binary H₂–THF clathrate hydrate,⁸ and is inadequate for the full complexity of the translational motions and their coupling to the rotations of the guest molecule. They can be treated properly only by solving numerically exactly the multidimensional Schrödinger equation for the coupled translation–rotation (T–R) motions. The quantum dynamics of a hydrogen molecule in confined geometries had been investigated previously for *p*- and *o*-H₂ on amorphous ice surfaces using quantum Monte Carlo simulations,²² and for H₂ within carbon nanotubes by means of quantum 4D calculations.^{23–25}

We have recently initiated a program of rigorous and comprehensive theoretical investigations of the quantum dynamics of hydrogen molecules inside the small and large cages of sII clathrate hydrate. Its objectives are 2-fold: to study dynamical features of direct experimental relevance, and to explore

[†] Part of the “Giacinto Scoles Festschrift”.

* Author to whom correspondence should be addressed. Electronic mail: zlatko.bacic@nyu.edu.

fundamental properties of highly quantum structured particles confined in cavities of different shapes and sizes. The initial publication²⁶ (paper I) reported the first quantum, fully coupled 5D calculations of the T–R eigenstates of a single H₂ molecule inside the small dodecahedral (5¹²) cage, which represented the first step toward achieving complete quantitative understanding of the quantum T–R dynamics of the guest molecule. In the second paper²⁷ (paper II), these calculations were extended to a D₂ molecule in the small cage. In addition, for one, two, and three *p*-H₂ and *o*-D₂ molecules in the small cage, the energetics and vibrationally averaged structural information were calculated rigorously using the diffusion Monte Carlo (DMC) method. In the third paper²⁸ (paper III), our focus shifted to the large hexakaidecahedral (5¹²6⁴) cage. For a single confined H₂ and D₂ molecule, the T–R energy levels and wave functions were calculated accurately in 5D utilizing the methodology developed in papers I and II. In addition, the DMC method was employed to determine the ground-state properties of one and two encapsulated *p*-H₂ and *o*-D₂ molecules. This study revealed large differences in the T–R dynamics of the hydrogen molecules inside the large and the small cages.

In this paper, the quantum T–R dynamics of a single hydrogen molecule in the small dodecahedral cage is investigated in considerably greater detail, involving a much larger number of T–R eigenstates, and substantially higher excitation energies than in paper I. The emphasis is on the T–R states of *p*-H₂ up to $\sim 380\text{ cm}^{-1}$ above the ground state, which includes also the $j = 2$ rotational level (at 356 cm^{-1} for the free H₂ molecule); in paper I, the analysis was limited to the 10 lowest *p*-H₂ T–R eigenstates with the excitation energies up to $\sim 200\text{ cm}^{-1}$ only. The behavior of the $j = 2$ rotational level in confinement, and the degree to which its 5-fold degeneracy is lifted by the anisotropy of the cage environment (as was shown in paper I to be the case for the 3-fold degenerate $j = 1$ rotational level) is of considerable interest, because the $j = 0 \rightarrow j = 2$ transition gives rise to the $S_0(0)$ roton peak present in the Raman spectra of the pure H₂² and the binary H₂–THF clathrate hydrate.⁸ The higher-lying T–R energy levels of *o*-D₂ are calculated and examined as well, but only for the purpose of studying how good a quantum number j is for the confined *p*-H₂ and *o*-D₂ at higher energies. In addition, the issues of (negative) anharmonicity of the translational modes, the strength of coupling between them, and the ability to assign the T–R states are investigated over a wider range of quantum numbers, in greater depth, and in more quantitative detail than in paper I. Finally, the average T–R energy of the encapsulated *p*-H₂ is calculated for the temperatures ranging from 0 to 150 K.

II. Theory

The methodology employed in this work was presented in paper I and used subsequently in papers II and III. Therefore, only its salient features are summarized here. The cage is assumed to be rigid, and the translation–rotation (T–R) eigenstates of the guest hydrogen molecule are calculated rigorously, as fully coupled. In papers I and II the framework O atoms of the small cage were arranged according to Patchkovskii and Tse,¹⁶ in the configuration which was close, but not identical, to that determined in the X-ray diffraction experiments.²⁹ In this work, the O atoms are placed in the experimentally determined positions,²⁹ for consistency with our studies in paper III involving the large cage. This slight change of the cage structure results in the T–R energy levels that differ by a few wave numbers from those reported in paper I, but the key characteristics of the quantum T–R dynamics elucidated in paper I are unaffected.

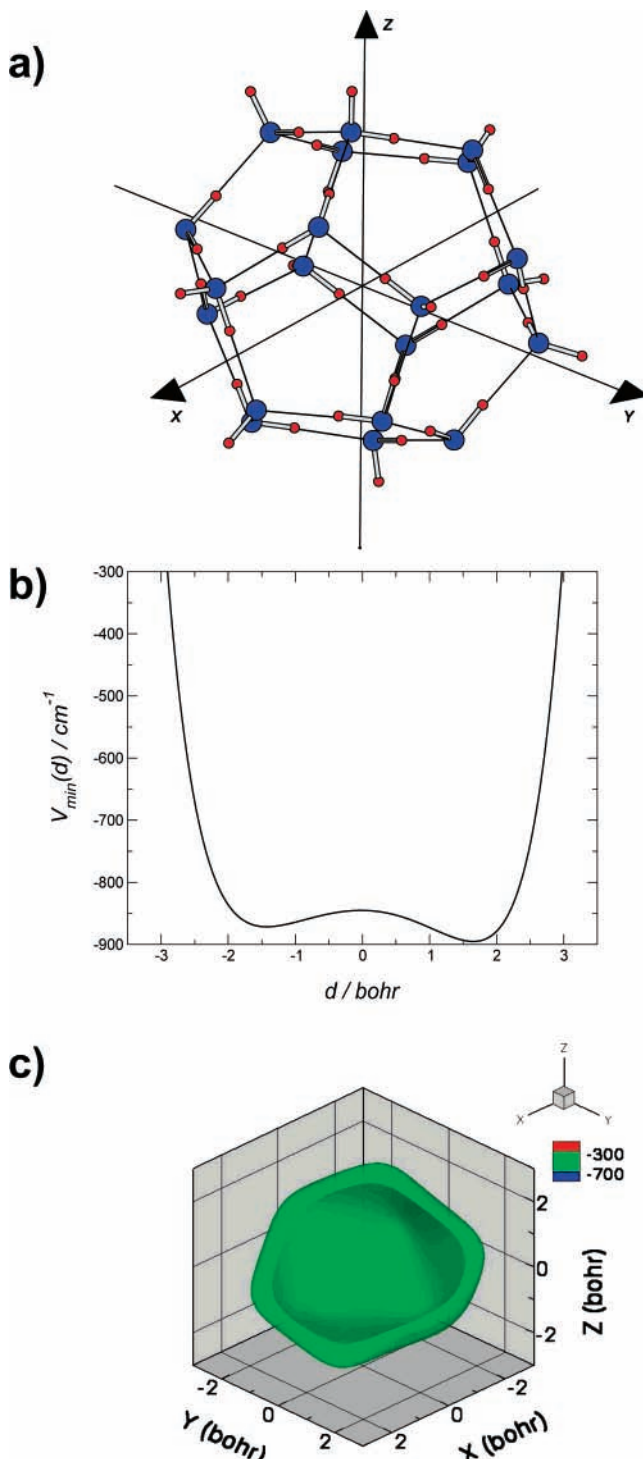


Figure 1. Small dodecahedral (5¹²) cage (a). The Cartesian x -, y -, z -coordinate axes coincide with the three principal axes of the cage. Shown in (b) is the one-dimensional cut through the 5D PES of H₂ in the small cage, along the line that connects the global minimum of the PES with the center of the cage. The 1D potential profile shown is obtained by minimizing the H₂–cage interaction with respect to the two angular coordinates of the H₂ molecule, at every position of its center of mass. In (c), two 3D isosurfaces are displayed for the H₂–cage PES, drawn at -700 and -300 cm^{-1} , respectively. They are generated in the same way as the 1D potential cut in (b).

The 20 O atoms occupy the corners of the dodecahedron (5¹²) shown in Figure 1a, which has 12 pentagonal faces. On each edge of the cage there is a hydrogen atom of a framework water molecule, forming a hydrogen bond between the two O atoms at the corners connected by the edge. However, these H atoms

are configurationally disordered. The Euler formula $F + V - E = 2$, where F , V , and E stand for the number of faces, vertices, and edges, respectively, applies to the clathrate hydrate cages, small and large. Because $F = 12$ and $V = 20$ for the small 5¹² cage, the number of edges (E) is 30. Hence, 10 water molecules must be double donors, whose both H atoms participate in the hydrogen bonds with two neighboring O atoms. The remaining 10 water molecules are single donors, with only one H atom in a hydrogen bond and the second O–H bond of the molecule free, pointing outward from the surface of the cage. It was mentioned in paper I that there are over 30 000 possible hydrogen-bonding topologies for a dodecahedral (H₂O)₂₀ cage.³⁰ The one used in paper I and here, shown in Figure 1a, was chosen at random by aiming to distribute the nonbonded O–H bonds rather evenly over the cage exterior. As a check, the bound-state calculations were performed for two additional hydrogen-bonding arrangements, yielding very similar results.

The 5D T–R energy levels and wave functions of a single H₂/D₂ molecule inside the cage, for the PES outlined below, are calculated as fully coupled using the approach presented in papers I and II. The set of five coordinates (x , y , z , θ , ϕ) is employed: x , y , and z are the Cartesian coordinates of the center of mass (c.m.) of the hydrogen molecule, and the two polar angles θ and ϕ specify its orientation. The coordinate system is aligned with the principal axes of the cage, and its origin is at the c.m. of the cage. The computational methodology relies on the 3D direct-product discrete variable representation (DVR)^{31,32} for the x -, y -, and z -coordinates and the spherical harmonics for the angular, θ - and ϕ -coordinates. The size of the final Hamiltonian matrix is drastically reduced by means of the sequential diagonalization and truncation procedure,^{31,33,34} without loss of accuracy. Diagonalization of this truncated Hamiltonian matrix yields the 5D T–R energy levels and wave functions. The dimension of the sine-DVR basis was 50 for each of the three Cartesian coordinates, and its grid spanned the range $-3.80 \text{ au} \leq \lambda \leq 3.80 \text{ au}$ ($\lambda = x, y, z$). The angular basis included functions up to $j_{\max} = 5$. The energy cutoff parameter for the intermediate 3D eigenvector basis³⁵ was set to 880 cm^{-1} for H₂ and 680 cm^{-1} for D₂, resulting in the final 5D Hamiltonian matrix of dimension 10 850 for H₂ and 16 500 for D₂. These basis set parameters were tested extensively for convergence. The rotational constants used in our calculations were $B_{\text{H}_2} = 59.322 \text{ cm}^{-1}$ and $B_{\text{D}_2} = 29.904 \text{ cm}^{-1}$.^{1,36,37}

The 5D PES for an H₂ molecule within the small cage was described already in papers I and II. It is pairwise additive, generated by summing over the interactions between the H₂ molecule and each of the 20 water molecules forming the cage; all the molecules are taken to be internally rigid. For the pair interaction between H₂ and H₂O we use the high-quality *ab initio* 5D (rigid monomer) PES for the H₂–H₂O complex by Hodges and co-workers,³⁸ with the global minimum at -240.8 cm^{-1} . One-dimensional cut through the 5D H₂-cage PES, plotted along the line connecting the global minimum of the PES with the cage center, is displayed in Figure 1b; it is generated by minimizing the H₂-cage interactions with respect to the angular coordinates θ and ϕ of the H₂ molecule, at every position of its center of mass. This plot shows that the PES is rather flat in the central region of the cage. The maximum at the center is only $\sim 50 \text{ cm}^{-1}$ higher than the global minimum lying at -895.22 cm^{-1} , which is much less than the ZPE of the T–R motions, 186.78 cm^{-1} . Consequently, this potential maximum has no visible impact on the T–R energy levels and wave functions. The 3D isosurfaces shown in Figure 1c convey the

TABLE 1: Translation–Rotation Energy Levels of the p-H₂ Molecule in the Small Dodecahedral Cavity of the Clathrate Hydrate, from the Quantum 5D Bound-State Calculations^a

<i>n</i>	ΔE	Δx	Δy	Δz	(v_x, v_y, v_z)	$c(0)$	$c(2)$
0	0.00	0.74	0.65	0.61	(0,0,0)		
1	52.64	1.18	0.63	0.57	(1,0,0)		
2	66.94	0.71	0.97	0.69	(0,1,0)		
3	82.45	0.66	0.73	0.91	(0,0,1)		
4	119.31	1.35	0.67	0.56	(2,0,0)		
5	130.99	1.10	0.92	0.67	(1,1,0)		
6	151.63	1.02	0.75	0.87	(1,0,1)		
7	154.63	0.69	1.15	0.70	(0,2,0)		
8	158.02	0.72	0.93	0.95	(0,1,1)		
9	184.37	0.64	0.74	1.07	(0,0,2)		
10	198.16	1.47	0.69	0.59	(3,0,0)		
11	206.51	1.29	0.97	0.62	(2,1,0)		
12	229.56	1.27	0.70	0.86	(2,0,1)		
13	231.11	1.08	0.96	0.82	(1,2,0)		
14	232.75	1.04	1.04	0.82	(1,1,1)		
15	246.80	0.61	1.24	0.89	(0,3,0)		
16	254.22	0.70	1.12	0.95	(0,2,1)		
17	267.59	0.88	0.92	0.96	(?, ?, ?)		
18	275.10	0.85	0.89	1.00	(?, ?, ?)		
19	287.41	1.52	0.77	0.62	(4,0,0)		
20	291.28	1.43	0.98	0.60	(3,1,0)		
21	299.85	0.64	0.74	1.19	(0,0,3)		
22	315.89	1.26	1.11	0.63	(2,2,0)		
23	316.46	1.40	0.70	0.89	(3,0,1)		
24	318.81	1.24	0.91	0.90	(2,1,1)	0.97	0.03
25	334.21	1.03	1.09	0.93	(1,2,1)	0.97	0.03
26	337.87	0.76	0.65	0.61	(0,0,0)	0.02	0.98 <i>j</i> = 2 [0.00]
27	339.29	0.77	0.66	0.61	(0,0,0)	0.02	0.98 <i>j</i> = 2 [1.42]
28	341.88	1.01	1.10	0.89	(1,3,0)	0.96	0.04
29	348.68	0.71	1.25	0.97	(0,4,0)	0.98	0.02
30	350.84	0.81	1.19	0.98	(?, ?, ?)	0.98	0.02
31	356.99	0.75	0.65	0.65	(0,0,0)	0.04	0.96 <i>j</i> = 2 [19.12]
32	359.20	1.16	0.79	0.98	(?, ?, ?)	0.94	0.06
33	363.52	0.87	1.12	0.96	(?, ?, ?)	0.98	0.02
34	378.66	0.82	0.66	0.60	(0,0,0)	0.01	0.99 <i>j</i> = 2 [40.79]
35	381.71	1.01	1.16	0.82	(?, ?, ?)	0.97	0.03
36	382.37	0.77	0.69	0.63	(0,0,0)	0.01	0.99 <i>j</i> = 2 [44.50]

^a They correspond to the $j = 0$ states of p-H₂, except those levels labeled $j = 2$. The excitation energies ΔE are relative to the ground-state energy $E_0 = -708.441 \text{ cm}^{-1}$. Also shown are the root-mean-square (rms) amplitudes Δx , Δy , and Δz (in au), and the Cartesian quantum number assignments (v_x, v_y, v_z). For the states $n = 24$ –36, the contributions to the wave functions from the $j = 0$ and $j = 2$ rotational basis functions, denoted $c(0)$ and $c(2)$, respectively, are displayed. For $n < 24$, $c(0) \geq 0.98$. The energies in [] brackets shown for the $j = 2$ states are relative to the lowest-energy $j = 2$ level, $n = 26$. All energies are in cm^{-1} . For additional explanation, see the text.

non-spherical shape of the potential experienced by H₂ inside the small cage.

III. Results and Discussion

The translation–rotation (T–R) levels of p-H₂ in the small dodecahedral cage with energies up to $\sim 380 \text{ cm}^{-1}$ above the ground state are given in Table 1, together with their root-mean-square (rms) amplitudes Δx , Δy , and Δz . The latter provide a measure of the wave function delocalization in the x -, y -, and z -directions, respectively, and are helpful in making the quantum number assignments. Listed next to them are the Cartesian (translational) quantum number assignments (v_x, v_y, v_z), for all the states where such assignment could be made. The states whose assignment is uncertain are designated (? , ?, ?). The assignments are discussed in more detail below.

The global minimum of the H₂-PES lies at -895.22 cm^{-1} . Because the ground-state energy of p-H₂ is -708.44 cm^{-1} , the zero-point energy (ZPE) is 186.78 cm^{-1} , or 20.9% of the well

TABLE 2: Higher-Lying Translation–Rotation Energy Levels $n = 15\text{--}40$ of the $o\text{-D}_2$ Molecule in the Small Dodecahedral Cavity of the Clathrate Hydrate, from the Quantum 5D Bound-State Calculations^a

n	ΔE	Δx	Δy	Δz	$c(0)$	$c(2)$	
15	151.83	0.58	1.10	0.83	0.94	0.06	
16	115.18	0.69	1.02	0.84	0.94	0.06	
17	162.65	0.95	0.82	0.83	0.93	0.07	
18	165.46	1.26	0.69	0.61	0.78	0.22	
19	166.15	0.81	0.60	0.54	0.09	0.91	$j = 2$
20	166.71	0.82	0.64	0.62	0.26	0.74	$j = 2$
21	167.59	0.84	0.81	0.83	0.78	0.22	
22	170.83	1.26	0.85	0.62	0.92	0.08	
23	182.81	0.71	0.58	0.58	0.02	0.98	$j = 2$
24	185.64	0.66	0.73	1.04	0.93	0.07	
25	186.64	1.17	0.88	0.71	0.92	0.08	
26	187.44	1.28	0.70	0.74	0.92	0.08	
27	190.99	1.11	0.89	0.78	0.92	0.08	
28	193.15	1.10	0.58	0.51	0.03	0.96	$j = 2$
29	194.38	1.08	0.59	0.52	0.04	0.95	$j = 2$
n	ΔE	Δx	Δy	Δz	$c(0)$	$c(2)$	
30	201.81	0.97	0.90	0.90	0.90	0.10	
31	204.06	0.78	0.82	0.66	0.23	0.77	$j = 2$
32	204.60	0.90	1.02	0.68	0.73	0.26	
33	206.78	0.72	0.80	0.62	0.03	0.97	$j = 2$
34	209.06	0.71	0.73	0.58	0.05	0.95	$j = 2$
35	212.59	0.79	0.96	0.88	0.75	0.25	
36	214.39	0.78	1.07	0.83	0.85	0.15	
37	214.66	0.75	0.84	0.65	0.25	0.75	$j = 2$
38	216.60	0.94	0.62	0.55	0.02	0.98	$j = 2$
39	216.77	1.08	0.78	0.87	0.91	0.09	
40	219.87	0.75	0.92	0.85	0.56	0.43	

^a The excitation energies ΔE (in cm^{-1}) are relative to the ground-state energy $E_0 = -742.039 \text{ cm}^{-1}$. Also shown are the root-mean-square (rms) amplitudes Δx , Δy , and Δz (in au), and the contributions to the wave functions from the $j = 0$ and $j = 2$ rotational basis functions, denoted $c(0)$ and $c(2)$, respectively. For $n < 15$, $c(0)$ is in the range 0.92–0.95. For those states where the dominant contribution is less than 0.90, both $c(0)$ and $c(2)$ are boldface. When $c(2) \geq 0.50$, the state is designated $j = 2$. For additional explanation, see the text.

depth. For $o\text{-D}_2$, the ground-state energy is -742.04 cm^{-1} , and the ZPE is 153.18 cm^{-1} , which represents 17.1% of the well depth.

A. How Good a Quantum Number Is j for $p\text{-H}_2$ and $o\text{-D}_2$ in the Small Cage? The last two columns in Table 1 show the contributions to the states $n = 24\text{--}36$ from the $j = 0$ and $j = 2$ rotational basis functions, denoted $c(0)$ and $c(2)$, respectively. They were obtained by projecting the eigenstates onto the rotational basis, taking the moduli squared and integrating over x , y , and z . For $n < 24$, $c(0) \geq 0.98$ and is not shown. One can see that for all the $j = 0$ states in Table 1, $c(0)$ is never less than 0.94. The five $j = 2$ states in Table 1, discussed below, are highly pure as well, with $c(2) \geq 0.96$. It is evident from these results that j remains to a high degree a good quantum number for both $j = 0$ and $j = 2$ states at the excitation energies well above those of the first ~ 10 excited T–R states of $p\text{-H}_2$ (and $o\text{-H}_2$) analyzed in paper I.

However, the same is not true for $o\text{-D}_2$ inside the small cage. In paper II, we reported that j was a good quantum number for the lowest ~ 10 excited T–R states of both $o\text{-D}_2$ and $p\text{-D}_2$. But this begins to break down as the excitation energies approach the $j = 2$ rotational level of the freely rotating $o\text{-D}_2$, 179.42 cm^{-1} . Table 2 lists the T–R eigenstates $n = 15\text{--}40$ whose energies, measured from the ground state, range from 150 to 220 cm^{-1} . Although for most of the states j is a good quantum number, a number of them, whether predominantly $j = 0$ [$c(0) \geq 0.50$] or $j = 2$ [$c(2) \geq 0.50$], show significant mixing of $j = 0$ and $j = 2$. They often appear as almost degenerate pairs of states, one primarily $j = 0$ and the other primarily $j = 2$;

examples of this are the states $n = 20$ and 21, $n = 31$ and 32, and $n = 36$ and 37. Others, like the state $n = 18$ in Table 2, which is predominantly $j = 0$ but with an appreciable $j = 2$ contribution, lie within 1 cm^{-1} of a $j = 2$ state. We suspect that these near-degeneracies between the (predominantly) $j = 0$ and $j = 2$ states are responsible for their mixed rotational character. This conjecture is supported by the fact that for $p\text{-H}_2$, where j is a good quantum number for the T–R states considered, nearly degenerate levels of this kind are not observed, as evident from Table 1. The most heavily rotationally mixed state in Table 2 is $n = 40$, with $j = 0$ and $j = 2$ contributing almost equally, 0.56 and 0.43, respectively. Thus, $p\text{-H}_2$ and $o\text{-D}_2$ confined to the small cage differ considerably in the extent to which j is a good quantum number, although there is little doubt that at higher excitation energies j will cease to be a good quantum number for $p\text{-H}_2$ as well.

B. Translational Mode Progressions. We now focus on the $j = 0$ states of $p\text{-H}_2$ in Table 1 and discuss first the T–R states corresponding to the pure x -, y -, and z -mode excitations, $(v_x, 0, 0)$, $(0, v_y, 0)$, and $(0, 0, v_z)$, respectively. States of this type with up to $v_x = v_y = 4$, and up to $v_z = 3$ have been identified; cf. Table 1. The translational parts of the wave functions of the x -mode states $(v_x, 0, 0)$ up to $v_x = 4$ are shown in Figure 2. The regular nodal patterns are evident in the 3D isosurface plots, making the quantum number assignment straightforward. The same holds for the wave functions of the y - and z -mode states, which are not shown. The energies of the x -, y -, and z -mode states listed in Table 1 are plotted in Figure 3 as a function of the number of quanta in each mode. This plot shows that in all three progressions, $(v_x, 0, 0)$, $(0, v_y, 0)$, and $(0, 0, v_z)$, the energy separation between the neighboring states increases with the number of quanta. Thus, the translational modes exhibit negative anharmonicity. This was established already in paper I, by comparing the energies of the fundamentals and the first overtones of the translational modes. The new results presented here demonstrate that the negative anharmonicity persists at higher levels of excitation. Also evident from Figure 3 is that the energy differences between the x -, y -, and z -mode states with the same number of quanta grow markedly with increasing excitation, with the x -mode states always having the lowest energy and the z -mode states the highest.

For the x -, y -, and z -mode progressions, Figure 4 displays the corresponding rms amplitudes Δx , Δy , and Δz as a function of the number of quanta in each mode. As expected, the three rms amplitudes grow with increasing v_x , v_y , and v_z , respectively; Δx is always the largest, implying that the potential is the softest in the x -direction. The rms amplitudes begin to level off for three and four quanta of excitation, indicating that the wave function delocalization has reached the limits imposed by the cage wall; see Figure 1b.

C. Translation Combination States, Mode Coupling, and Assignments. Next we discuss the $j = 0$ combinations states of $p\text{-H}_2$ where any two, or all three, translational modes are excited. Most such states in Table 1 have wave functions that are sufficiently regular so that their assignment is not in doubt. Typical examples are displayed in Figure 5 showing the translational parts of the wave functions of the states $n = 22$ $(2, 2, 0)$, $n = 24$ $(2, 1, 1)$, $n = 25$ $(1, 2, 1)$, and $n = 28$ $(1, 3, 0)$. These plots also illustrate some of the ways in which the wave functions of these higher-lying states, though assignable, are distorted as a result of the coupling among the translational modes. The mode coupling manifests itself also in the energies of the combination states. If the translational modes were completely uncoupled, the excitation energy of the combination

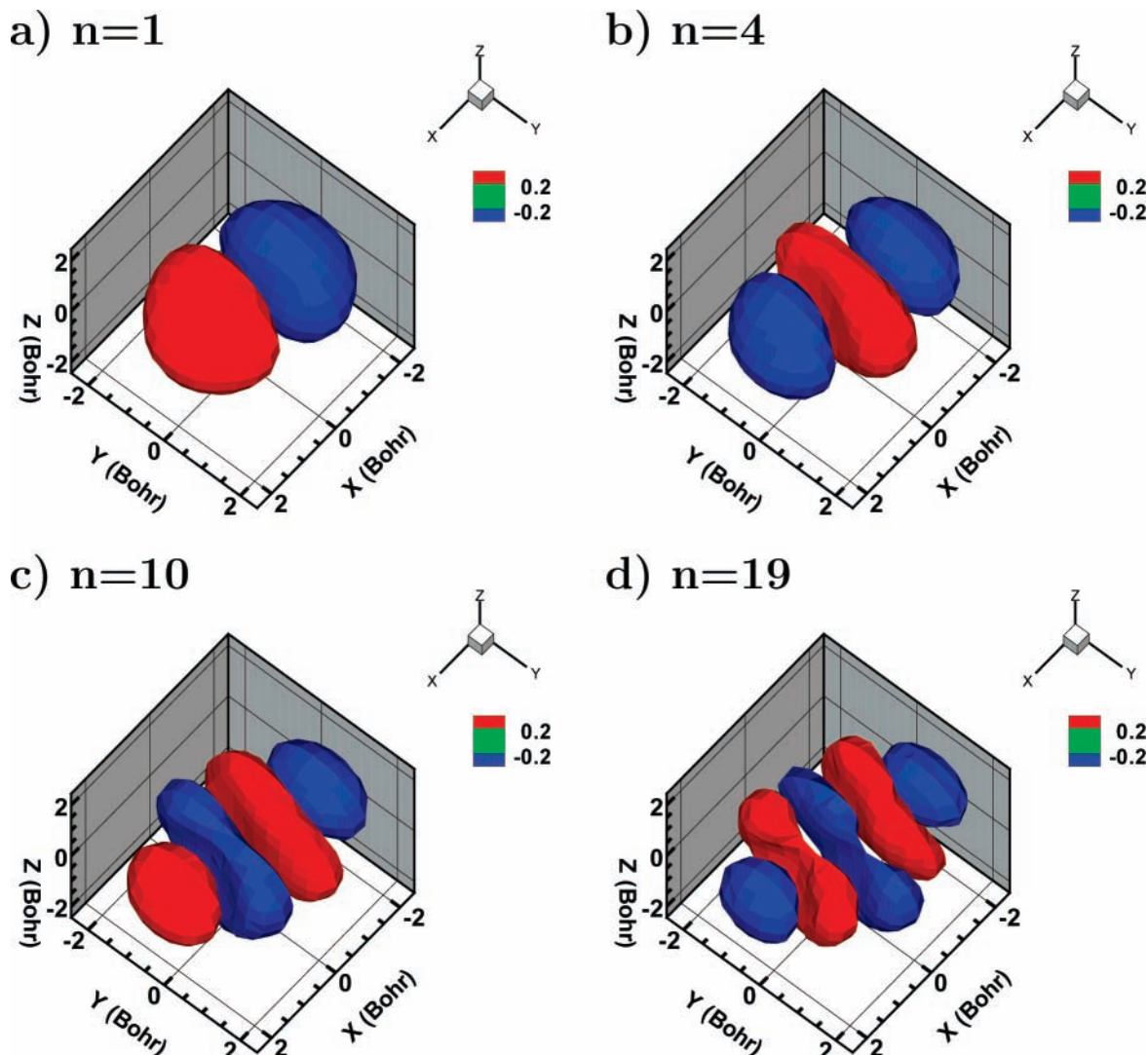


Figure 2. 3D isosurfaces of the translational components of the wave functions of the $j = 0$ p -H₂ states (a) $n = 1$ (1, 0, 0), (b) $n = 4$ (2, 0, 0), (c) $n = 10$ (3, 0, 0), and (d) $n = 19$ (4, 0, 0), listed in Table 1.

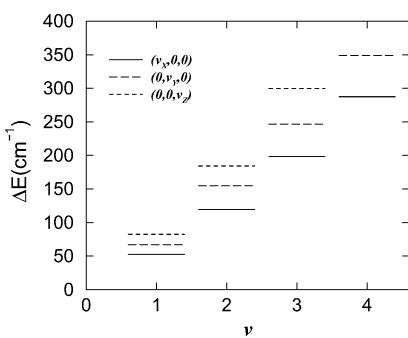


Figure 3. Excitation energies ΔE of the x -, y -, and z -mode states $(\nu_x, 0, 0)$, $(0, \nu_y, 0)$, and $(0, 0, \nu_z)$, respectively, vs the number of quanta ν in each mode.

state (ν_x, ν_y, ν_z) would be equal to the sum of the energies of the pure x -, y -, and z -mode excitations $(\nu_x, 0, 0)$, $(0, \nu_y, 0)$, and $(0, 0, \nu_z)$, respectively. A closer look at the results in Table 1 shows that this is not the case. We define ΔE_{nonadd} as

$$\Delta E_{\text{nonadd}} = \Delta E_{\nu_x, \nu_y, \nu_z} - [\Delta E_{\nu_x, 0, 0} + \Delta E_{0, \nu_y, 0} + \Delta E_{0, 0, \nu_z}] \quad (1)$$

to serve as a rough indicator of the strength of the mode coupling in the state (ν_x, ν_y, ν_z) . The excitation energies of the states

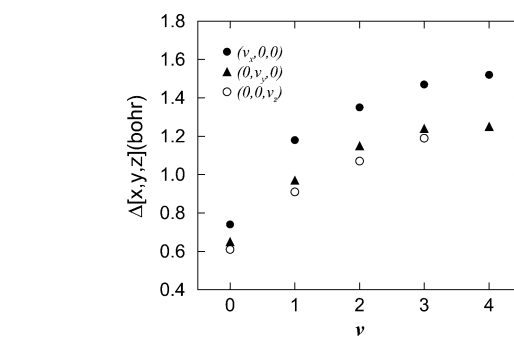


Figure 4. Root-mean-square amplitudes Δx , Δy , and Δz of the states $(\nu_x, 0, 0)$, $(0, \nu_y, 0)$, and $(0, 0, \nu_z)$, respectively, vs the number of quanta ν in each mode.

appearing in eq 1 are those given in Table 1. Figure 6 shows ΔE_{nonadd} for the states $(\nu_x, 1, 0)$, $(\nu_x, 0, 1)$, and $(\nu_x, 1, 1)$, with $\nu_x = 1, 2, 3$. Several trends are apparent. For the states $(\nu_x, 1, 0)$ and $(\nu_x, 0, 1)$ considered, ΔE_{nonadd} ranges from 10 to 50 cm^{-1} , which amounts to 9–12% of the excitation energies; these percentages are higher for the states $(\nu_x, 1, 1)$, where they are 13% for $\nu_x = 1$ and 16% for $\nu_x = 2$. For each of the three progressions, ΔE_{nonadd} grows with increasing ν_x , consistent with the notion that the mode coupling becomes stronger at higher energies. For a given ν_x , ΔE_{nonadd} is greater for the state

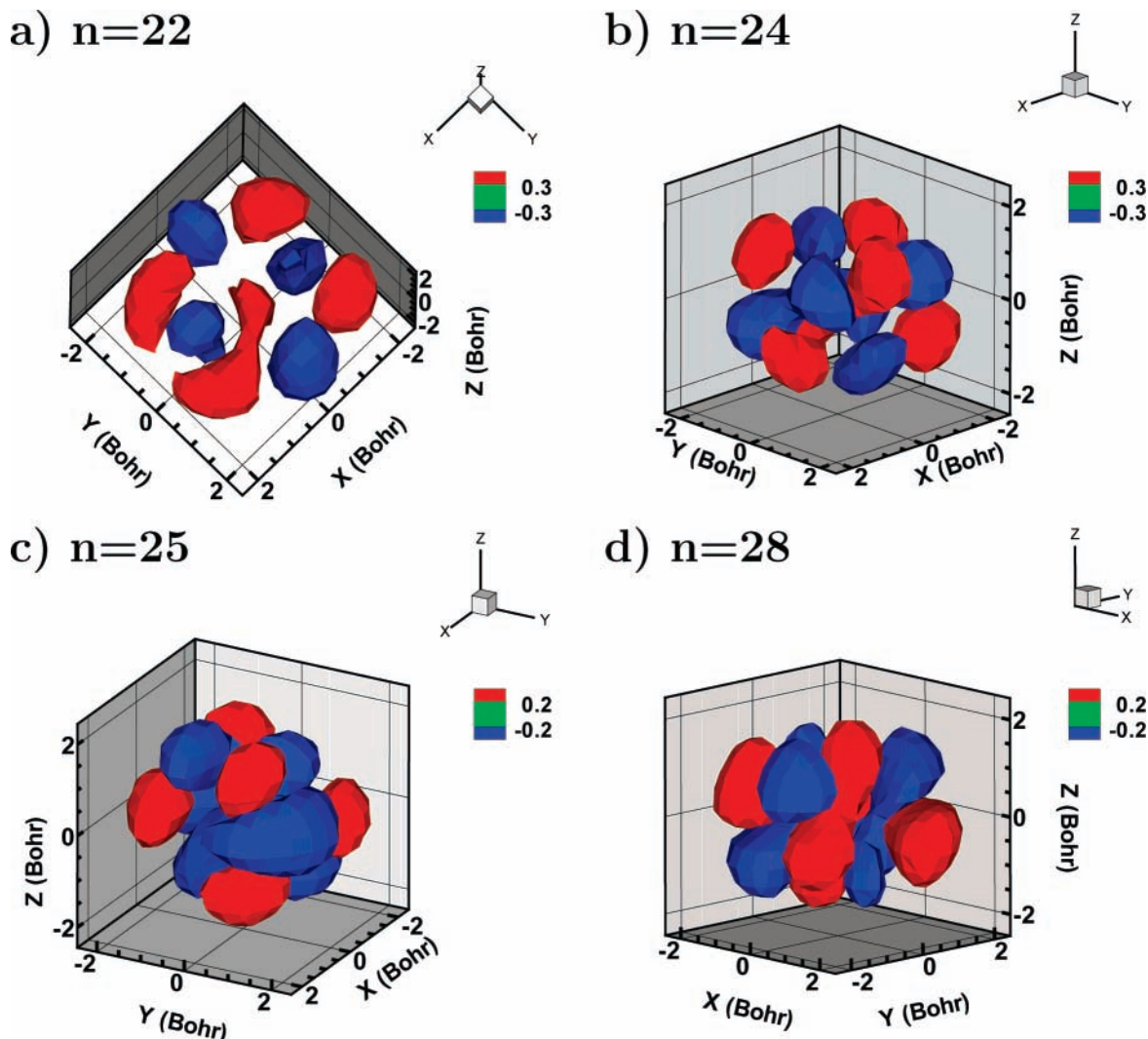


Figure 5. 3D isosurfaces of the translational components of the wave functions of the $j = 0$ p -H₂ states (a) $n = 22$ (2, 2, 0), (b) $n = 24$ (2, 1, 1), (c) $n = 25$ (1, 2, 1), and (d) $n = 28$ (1, 3, 0), listed in Table 1.

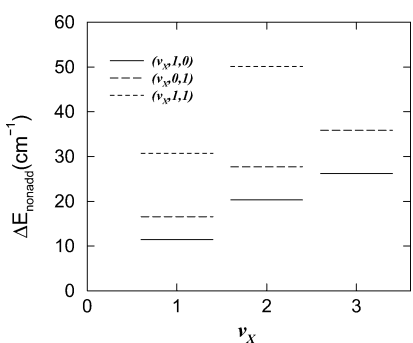


Figure 6. ΔE_{nonadd} defined in eq 1, for selected translational combination states, as a function of ν_x . For additional explanation, see the text.

($\nu_x, 0, 1$) than for the state ($\nu_x, 1, 0$), suggesting that the x -mode couples more strongly to the z -mode than to the y -mode. ΔE_{nonadd} is the largest for the state ($\nu_x, 1, 1$), which has the highest energy for a given ν_x . These observations hold also for the other combination states in Table 1, which do not appear in Figure 6. Thus, for the states (1, 2, 0) and (2, 2, 0), ΔE_{nonadd} is 23.84 cm^{-1} (10.3%) and 41.95 cm^{-1} (13.3%), respectively; for the states (0, 2, 1) and (1, 2, 1), ΔE_{nonadd} is 17.14 cm^{-1} (6.7%) and 44.59 cm^{-1} (13.3%), respectively.

In the case of a number of $j = 0$ states in Table 1 the Cartesian quantum number assignments could not be done with confi-

dence, hence their designation (? , ?, ?). The two lowest-energy unassigned states are $n = 17$ and $n = 18$, and the translational parts of their wave functions can be seen in Figure 7. The appearance of the two wave functions, especially for $n = 18$, energy considerations, and the trends in the rms amplitudes lead one to conclude that both states have two quanta in the z -mode and one quantum in either x - or y -mode. But, the wave functions are distorted and tilted relative to all three Cartesian axes, evidence of strong coupling among the translational modes, making the assignment problematic. For the state $n = 30$, the nodal pattern of the wave function shown in Figure 7, the energy of the state relative to those of the states $n = 17$ and $n = 18$, and the large value of Δ_y suggest a very tentative (0, 2, 2) assignment. The same reasoning, and the large value of Δ_x , lead to a plausible assignment of the state $n = 32$ as (2, 0, 2); its wave function is also shown in Figure 7.

The translational parts of the wave functions of the states $n = 33$ and $n = 35$ are shown in Figure 8. Their appearance and the information about these states in Table 1 provided no basis for even a tentative assignment. It is conceivable that the assignment of the translational modes might be possible by plotting the wave functions in coordinates other than Cartesian, e.g., spherical polar, cylindrical, or other, but this was not pursued.

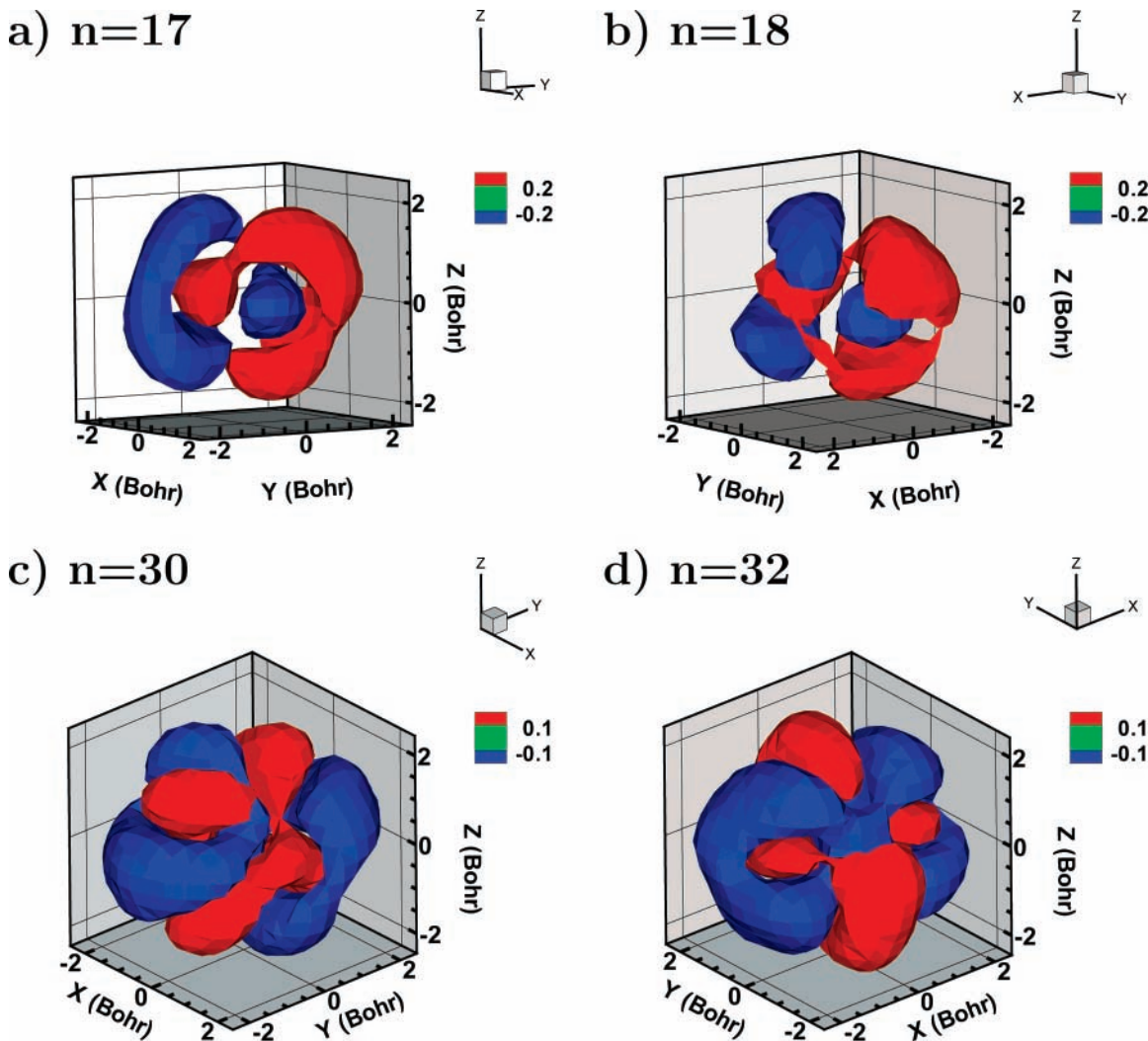


Figure 7. 3D isosurfaces of the translational components of the $j = 0$ p -H₂ states (a) $n = 17$, (b) $n = 18$, (c) $n = 30$, and (d) $n = 32$, listed in Table 1. Tentative assignments of these states are discussed in the text.

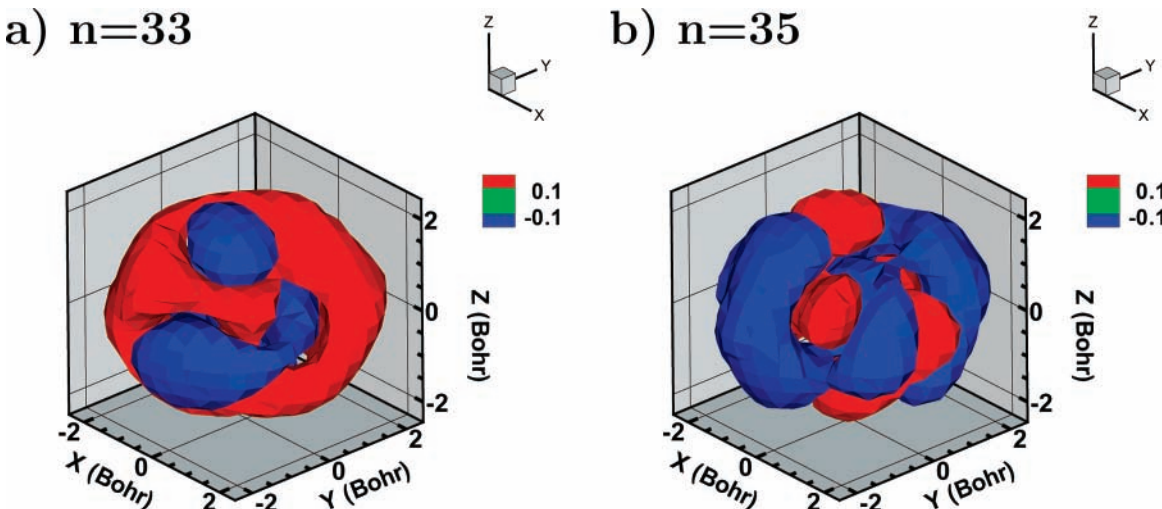


Figure 8. 3D isosurfaces of the translational components of the $j = 0$ p -H₂ states (a) $n = 33$ and (b) $n = 35$, listed in Table 1.

D. $j = 2$ States of the Encapsulated p -H₂. In papers I and II we reported that the anisotropy of the environment lifted completely the 3-fold degeneracy of the $j = 1$ rotational level of o -H₂ and p -D₂, respectively, confined in the small cage. Moreover, the $j = 1$ level splittings were found to be remarkably

similar for o -H₂ and p -D₂,²⁷ which was explained in terms of a simple 2D model developed in paper I.

Table 1 shows that the 5-fold degeneracy of the $j = 2$ level of p -H₂ is lifted fully as well. There are five $j = 2$ states ($n = 26, 27, 31, 34, 36$), all in the ground translational state

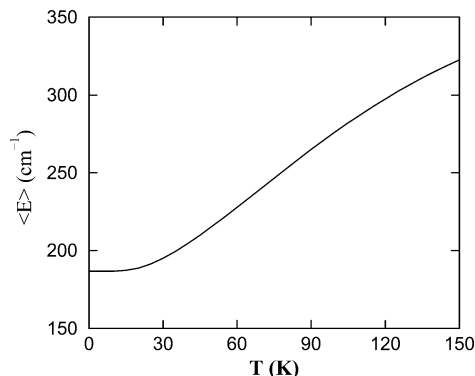


Figure 9. Temperature dependence of the average energy $\langle E \rangle$ for $p\text{-H}_2$ in the small cage. For additional explanation, see the text.

(0, 0, 0); the lowest-energy state $n = 26$ and the highest-energy state $n = 36$ are 44.50 cm^{-1} apart. The pattern of these five $j = 2$ states is interesting. The state $n = 31$ at 356.99 cm^{-1} is just 1 cm^{-1} higher in energy than the $j = 2$ level of the free $p\text{-H}_2$ molecule, which lies at $6B = 355.93\text{ cm}^{-1}$. The four remaining $j = 2$ states form two closely spaced pairs: $n = 26$ and $n = 27$, differing by 1.4 cm^{-1} , lie $\sim 19\text{ cm}^{-1}$ below $n = 31$, and $n = 34$ and $n = 36$, 3.7 cm^{-1} apart, are $\sim 25\text{ cm}^{-1}$ above $n = 31$.

Raman spectra of the pure hydrogen hydrate² show molecular hydrogen roton peaks $S_0(0)$, $S_0(1)$, and $S_0(2)$ at 355 , 590 , and 815 cm^{-1} , respectively. They correspond to $\Delta j = 2$ transitions out of $j = 0$, 1 , and 2 rotational levels, respectively, of the H_2 molecule. The same roton peaks were measured also for the binary $\text{H}_2\text{-THF}$ clathrate hydrate.⁸ Clearly, the roton peak observed at 355 cm^{-1} falls in the middle of our five $j = 2$ states in Table 1 and nearly coincides with the state $n = 31$ at 357 cm^{-1} . Further analysis is required to clarify the relationship between our results and the Raman spectra.

E. Temperature Dependence of the Average Energy. The energy levels listed in Table 1 allow us to calculate the temperature dependence of various quantities of interest. One of them is the average translation–rotation energy $\langle E \rangle$ of the encapsulated $p\text{-H}_2$ at the temperature T , given by

$$\langle E \rangle = \sum_n p_n E_n \quad (2)$$

where E_n are the T–R energy levels of $p\text{-H}_2$ in Table 1 and p_n is given by the well-known expression

$$p_n = \frac{e^{-E_n/kT}}{\sum_n e^{-E_n/kT}} \quad (3)$$

with k representing the Boltzmann constant.

Figure 9 displays $\langle E \rangle$ in the temperature range 0–150 K. At 0 K, $\langle E \rangle$ is equal to the ZPE of 186.78 cm^{-1} , because only the ground state is occupied. Above 15 K, excited T–R states begin to be populated and $\langle E \rangle$ increases with the temperature. At 150 K, the probability of being in the ground state is down to 17.5% (at 100 K, it is 29.9%) vs 10.6% for the first excited state, and $\langle E \rangle$ reaches 320 cm^{-1} .

IV. Conclusions

We have reported a rigorous study of the quantum T–R dynamics of a single $p\text{-H}_2$ molecule inside the small dodecahedral cage of the SII clathrate hydrate. The present investigation

extends to considerably higher excitation energies, and covers a much larger number of T–R energy levels, than our previous study of this system.²⁶ The higher-lying T–R eigenstates of $p\text{-H}_2$, as well as those of $o\text{-D}_2$, were calculated rigorously, as fully coupled in 5D, and the cage was taken to be rigid, employing the computational methodology developed and implemented by us earlier.^{26–28} They span the energy range that for both $p\text{-H}_2$ and $o\text{-D}_2$ includes their respective $j = 2$ rotational levels; this was not the case previously.^{26,27} Careful analysis of the T–R states of $p\text{-H}_2$ up to $\sim 380\text{ cm}^{-1}$ relative to the ground state showed that j is to a high degree a good quantum number for both $j = 0$ and $j = 2$ eigenstates in this energy range. However, this does not hold true for the confined $o\text{-D}_2$ at the excitation energies comparable to the $j = 2$ rotational level of the free molecule, 179 cm^{-1} , where a number of T–R states exhibit significant mixing of $j = 0$ and $j = 2$ rotational basis functions.

Our study found that the anisotropy of the cage environment completely lifts the 5-fold degeneracy of the $j = 2$ level of $p\text{-H}_2$, just as it does for the triply degenerate $j = 1$ level of $o\text{-H}_2$.²⁶ The five $j = 2$ states, all in the ground translational state, are spread over 44.5 cm^{-1} . The middle $j = 2$ state at 357 cm^{-1} is very close in energy to the $S_0(0)$ roton peak observed at 355 cm^{-1} in the Raman spectra of the pure hydrogen hydrate.² Further work is needed to firmly establish the connection between the theoretical results and Raman spectroscopy.

Pure translational x -, y -, and z -mode excitations of $p\text{-H}_2$ were identified with up to four quanta in each mode (three in the case of the z -mode). Their nodal patterns are regular, allowing easy quantum number assignment. In all three progressions, the energy separation between the neighboring states increases with the number of quanta, showing that the translational modes continue to exhibit pronounced negative anharmonicity at the levels of excitation considerably higher than those examined previously.²⁶

The $j = 0$ combination states of $p\text{-H}_2$, where two or all three translational modes are excited, were studied in considerable detail with respect to their assignability and the extent of the mode coupling as a function of the excitation energy. For most, but not all, of the T–R states considered, the translational wave functions are sufficiently regular to permit the states to be assigned with reasonable confidence, despite various types of distortions of the nodal patterns due to the mode coupling. The mode coupling is reflected also in the excitation energies of the combination states, which are typically ~ 9 – 15% higher than the sum of the corresponding pure x -, y -, and z -mode excitations.

The average energy of the encapsulated $p\text{-H}_2$ was determined in the temperature range 0–150 K, utilizing the calculated T–R energy levels.

Our results were obtained for the well-defined pairwise additive model of the interaction between the H_2 molecule and the cage, which is treated as rigid. We believe that the picture of the quantum T–R dynamics that emerges from them is qualitatively, and at least semiquantitatively, correct. Nevertheless, it is desirable to go beyond these assumptions to assess their effects, although this is not an easy task. The calculation of a more accurate, nonadditive 5D PES for H_2 interacting with the framework of hydrogen-bonded H_2O molecules poses a serious challenge. The same holds for allowing the cages, small and large, to be flexible while maintaining the present high level of treatment of the quantum dynamics of the guest hydrogen molecule. Much of our future effort will be directed toward these two goals.

Acknowledgment. Z.B. is grateful to the National Science Foundation for partial support of this research, through Grant CHE-0315508. The computational resources used in this work were funded in part by the NSF MRI grant CHE-0420870. Acknowledgment is made to the donors of the American Chemical Society Petroleum Research Fund for partial support of this research.

References and Notes

- (1) Sloan, E. D. *Clathrate hydrates of natural gases*; Marcel Dekker: New York, 1998.
- (2) Mao, W. L.; Mao, H. K.; Goncharov, A. F.; Struzhkin, V. V.; Guo, Q.; Hu, J.; Shu, J.; Hemley, R.; Somayazulu J. M. and Y. Zhao, *Science* **2002**, *297*, 2247.
- (3) Mao, W. L.; Mao, H. K. *Proc. Natl. Acad. Sci. U.S.A.* **2004**, *101*, 708.
- (4) Fichtner, M. *Adv. Eng. Mater.* **2005**, *7*, 443.
- (5) Hu, Y. H.; Ruckenstein, E. *Angew. Chem., Int. Ed.* **2006**, *45*, 2011.
- (6) Lokshin, K. A.; Zhao, Y.; He, D.; Mao, W. L.; Mao, H. K.; Hemley, R. J.; Lobanov, M. V.; Greenblatt, M. *Phys. Rev. Lett.* **2004**, *93*, 125503.
- (7) Zhao, Y.; Xu, H.; Daemen, L. L.; Lokshin, K.; Tait, K. T.; Mao, W. L.; Luo, J.; Currier, R. P.; Hickmott, D. D. *Proc. Natl. Acad. Sci. U.S.A.* **2007**, *104*, 5727.
- (8) Florusse, L. J.; Peters, C. J.; Schoonman, J.; Hester, K. C.; Koh, C. A.; Dec, S. F.; Marsh, K. N.; Sloan, E. D. *Science* **2004**, *306*, 469.
- (9) Lee, H.; Lee, J.-W.; Kim, D. Y.; Park, J.; Seo, Y.-T.; Zeng, H.; Moudrakovski, I. L.; Ratcliffe, C. J.; Ripmeester, J. A. *Nature* **2005**, *434*, 743.
- (10) Kim, D. Y.; Lee, H. *J. Am. Chem. Soc.* **2005**, *127*, 9996.
- (11) Hester, K. C.; Strobel, T. A.; Sloan, E. D.; Koh, C.; Huq, A. A.; Schultz, A. J. *J. Phys. Chem. B.* **2006**, *110*, 14024.
- (12) Strobel, T. A.; Taylor, C. J.; Hester, K. C.; Dec, S. F.; Koh, C. A.; Miller, K. T.; Sloan, E. D., Jr. *J. Phys. Chem. B.* **2006**, *110*, 17121.
- (13) Choi, Y. N.; Yeon, S. H.; Park, Y.; Choi, S.; Lee, H. *J. Am. Chem. Soc.* **2007**, *129*, 2208.
- (14) Anderson, R.; Chapoy, A.; Tohidi, B. *Langmuir* **2007**, *23*, 3440.
- (15) Sluiter, M. H. F.; Belosludov, R. V.; Jain, A.; Belosludov, V. R.; Adachi, H.; Kawazoe, Y.; Higuchi, K.; Otani, T. *Lect. Notes Comput. Sci.* **2003**, *2858*, 330.
- (16) Patchkovskii, S.; Tse, J. S. *Proc. Natl. Acad. Sci. U.S.A.* **2003**, *100*, 14645.
- (17) Patchkovskii, S.; Yurchenko, S. N. *Phys. Chem. Chem. Phys.* **2004**, *6*, 4152.
- (18) Alavi, S.; Ripmeester, J. A.; Klug, D. D. *J. Chem. Phys.* **2005**, *123*, 024507.
- (19) Inerbaev, T. M.; Belosludov, V. R.; Belosludov, R. V.; Sluiter M.; Kawazoe, Y. *Comput. Mater. Sci.* **2006**, *36*, 229.
- (20) Lee, J. W.; Yedlapalli, P.; Lee, S. J. *Phys. Chem. B.* **2006**, *110*, 2332.
- (21) Alavi, S.; Ripmeester, J. A.; Klug, D. D. *J. Chem. Phys.* **2006**, *124*, 014704.
- (22) Buch, V.; Devlin, J. P. *J. Chem. Phys.* **1993**, *98*, 4195.
- (23) Lu, T.; Goldfeld, E. M.; Gray, S. K. *J. Phys. Chem. B.* **2003**, *107*, 12989.
- (24) Lu, T.; Goldfeld, E. M.; Gray, S. K. *J. Phys. Chem. B.* **2006**, *110*, 1742.
- (25) Yildirim, T.; Harris, A. B. *Phys. Rev. B* **2003**, *67*, 245413.
- (26) Xu, M.; Elmatad, Y.; Sebastianelli, F.; Moskowitz, J. W.; Bačić, Z. *J. Phys. Chem. B.* **2006**, *110*, 24806.
- (27) Sebastianelli, F.; Xu, M.; Elmatad, Y.; Moskowitz, J. W.; Bačić, Z. *J. Phys. Chem. C.* **2007**, *111*, 2497.
- (28) Sebastianelli, F.; Xu, M.; Kanan, D. K.; Bačić, Z. *J. Phys. Chem. A.* **2007**, *111*, 6115.
- (29) Mak, T. C. W.; McMullan, R. K. *J. Chem. Phys.* **1965**, *42*, 2732.
- (30) McDonald, S.; Ojamäe, L.; Singer, S. J. *J. Phys. Chem. A.* **1998**, *102*, 2824.
- (31) Bačić Z.; Light, J. C. *Annu. Rev. Phys. Chem.* **1989**, *40*, 469.
- (32) Mandziuk, M.; Bačić, Z. *J. Chem. Phys.* **1993**, *98*, 7165.
- (33) Bačić, Z.; Light, J. C. *J. Chem. Phys.* **1986**, *85*, 4594.
- (34) Bačić, Z.; Light, J. C. *J. Chem. Phys.* **1987**, *86*, 3065.
- (35) Liu, S.; Bačić, Z.; Moskowitz, J. W.; Schmidt, K. E. *J. Chem. Phys.* **1995**, *103*, 1829.
- (36) Jankowski, P.; Szalewicz, K. *J. Chem. Phys.* **1998**, *108*, 3554.
- (37) Jankowski, P.; Szalewicz, K. *J. Chem. Phys.* **2005**, *123*.
- (38) Hodges, M. P.; Wheatley, R. J.; Schenter, G. K.; Harvey, A. H. *J. Chem. Phys.* **2004**, *120*, 710.